Influence of the charge carrier tunneling processes on the recombination dynamics in single lateral quantum dot molecules

C. Hermannstädter,[1,*] G. J. Beirne,[1,†] M. Witzany,[1] M. Heldmaier,[1] J. Peng,[2] G. Bester,[2] L. Wang,[2,3] A. Rastelli,[3] O. G. Schmidt,[3] and P. Michler[1]

[1]*Institut für Halbleiteroptik und Funktionelle Grenzflächen, Universität Stuttgart, Allmandring 3, 70569 Stuttgart, Germany*

[2]*Max-Planck-Institut für Festkörperforschung, Heisenbergstr. 1, 70569 Stuttgart, Germany*

[3]*Institut für Integrative Nanowissenschaften, IFW Dresden, Helmholtzstr. 20, 01069 Dresden, Germany*

(Received 9 November 2009; revised manuscript received 22 April 2010; published 10 August 2010)

We report on the charge carrier dynamics in single lateral quantum dot molecules and the effect of an applied electric field on the molecular states. Controllable electron tunneling manifests itself in a deviation from the typical excitonic decay behavior in dot molecules. It results in a faster population decay and can be strongly influenced by the tuning electric field and intermolecular Coulomb energies. A rate equation model is developed and compared to the experimental data to gain more insight into the charge transfer and tunneling mechanisms. Nonresonant (phonon-mediated) electron tunneling which changes the molecular exciton character from direct to indirect, and vice versa, is found to be the dominant tunable decay mechanism of excitons besides radiative recombination.

DOI: 10.1103/PhysRevB.82.085309 PACS number(s): 78.67.Hc, 73.21.La, 78.55.Cr

I. INTRODUCTION

The charge carrier configuration and dynamics in coupled quantum dot (QD) systems are the essential properties that need to be understood in order to gain the ability to coherently manipulate the coupling in the system using external electric, magnetic, or light fields. This degree of control over the QD system represents an essential step toward the realization of quantum gates. Over the last years, optically addressable self-assembled semiconductor single QDs have been presented as sources for triggered single photons and polarization-entangled photon pairs,[1–5] and first quantum gates have been demonstrated.[6,7] Such QDs can be assembled to larger molecular structures by vertically stacking them along the growth direction[8–14] and laterally arranging them.[15–17] A recent demonstration on a vertical QD molecule (QDM) has shown conditional quantum dynamics with one QD state being controlled via the other one.[18] The static properties of different types of QDMs, such as their coupling mechanisms and electronic structure, as well as their light emission properties have been extensively experimentally studied and theoretically described.[10–12,19–21] A detailed dynamical analysis of the coupling in lateral QDMs using time-resolved spectroscopic methods, however, has not yet been done. As previously reported in Refs. 17, 20, and 21, the dominant coupling mechanism in lateral double dots is electronic tunneling, which strongly depends on the charge carriers' effective masses, the excitonic binding energies and the potential landscape. It is therefore of particular interest to study the dependence of the tunnel dynamics on these parameters, especially considering the long-term objective of gaining the ability to control them in a deterministic way.

In this paper we present results on the charge carrier and exciton dynamics of laterally coupled QDs which highlight the significant difference to single dots and vertical QDMs as well as the important impact of an external electric field. Using a rate equation model and a phenomenological explanation of the underlying physical processes, the experimental data are described qualitatively as well as quantitatively with a set of parameters obtained from fits to the data. We discuss the peculiar properties of the investigated molecules and the arising consequences for possible future application in quantum information processing.

II. LATERAL QUANTUM DOT MOLECULES

A. Fabrication and structural parameters

The investigated lateral QDMs consist of two $In_xGa_{1-x}As$ QDs that form on top of a "basin" filled with $In_yGa_{1-y}As$ and are grown by molecular-beam epitaxy combined with *in situ* selective etching.[16] Both the dots and the basin exhibit gradients in the In content, x, y, especially in the growth direction (for further details see Refs. 20 and 21). Furthermore all QDMs are aligned along the same crystallographic axis $[1\bar{1}0]$, as displayed in the atomic force micrograph (AFM) in Fig. 1(a) and presented in Ref. 17. This alignment allows one to apply lateral electric fields via parallel electrodes on top of the sample, which are fabricated using photolithography and vapor phase deposition. As described in detail in Ref. 20 these lateral QDMs have a typical height of 2.5 nm, width of 40–48 nm, and edge-to-edge distance of 4–8 nm [see Fig. 1(b)].

The QDMs, with a spatial density of about 10^8 cm^{-2}, were placed inside a low Q planar cavity to obtain a higher

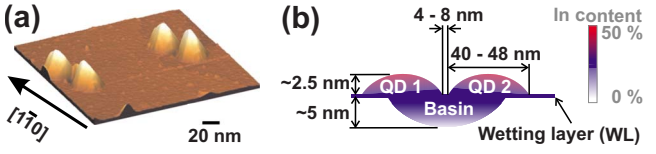

FIG. 1. (Color online) (a) AFM image showing two uncapped lateral QDMs and their orientation along the $[1\bar{1}0]$ crystal direction. (b) Schematic picture illustrating the typical dimensions and composition of the lateral QDMs.

photoluminescence (PL) collection efficiency and thus an enhanced signal-to-noise ratio at the typical emission energies of around 1.35 eV. This was required to simultaneously resolve the excitonic emission both spectrally and temporally. A detailed description of the structure under investigation is given in Ref. 22 including the demonstration of quantum coupling via photon cross-correlation spectroscopy.

A theoretical description of these special lateral QDMs is given in Ref. 21. Therein, a discussion is carried out concerning the electronic level structure of single particles and correlated excitons, the PL resulting from neutral excitonic decay, the tunability via lateral electric fields, as well as the charge carrier capture processes for nonresonant excitation. The discussed lateral QDM exhibits a unique potential landscape and energy-level structure which accounts for the dots forming the QDM and the overgrown In-rich basin (Fig. 6 in Ref. 21). The confined electron—treated as a single-particle—feels the whole QDM as one compound object in which it can easily tunnel between both dots constituting the molecule. This tunnel coupling is possible, even at the large center-to-center distance between the two dots, due to the narrow GaAs interdot barrier and the effect of the overgrown basin. Consequently, the electron spatial distribution in the QDM can be tuned using lateral electric fields, i.e., it can be either completely shifted to one of the dots or equally distributed over the whole QDM. This state of maximum electron coupling is referred to as electron alignment and is achieved at the electron alignment field F_e. The hole, however, feels the QDM as two rather separated dots and thus remains almost completely localized in either of the dots. It shows no significant tunnel coupling.

B. Microphotoluminescence spectroscopy

For the measurements that are presented here, the sample was mounted in a low-temperature (5 K) micro-PL setup with a focus diameter of about 1 μm. The low spatial density of the investigated QDM samples directly allows for the examination of one single QDM at a time. It furthermore ensures that the main part of the photogenerated electron-hole pairs under nonresonant excitation is captured by the investigated QDM. The optical excitation was performed using a 3 ps pulsed Ti:sapphire laser which nonresonantly pumps the QDM via the surrounding bulk GaAs barrier and the wetting layer (WL). The excitation powers are chosen slightly below or around the neutral exciton saturation level (300 W/cm^2) such that the maximum PL signal could be obtained. Consequently, the examined QDM is on average occupied by one to two electron-hole pairs per excitation cycle. Due to this moderate charge carrier population of the QDM and the suppression of surface-enhanced processes in overgrown QD structures, recombination mechanisms other than radiative decay, such as Auger-type processes, do not play a significant role.

The QDM PL was dispersed using a 0.3 m spectrometer with a 1200 l/mm grating resulting in a theoretical Fourier transform limited spectral resolution of approximately 0.2 meV and a temporal resolution of 40 ps, which was experimentally verified by measuring the 3 ps laser pulses. The

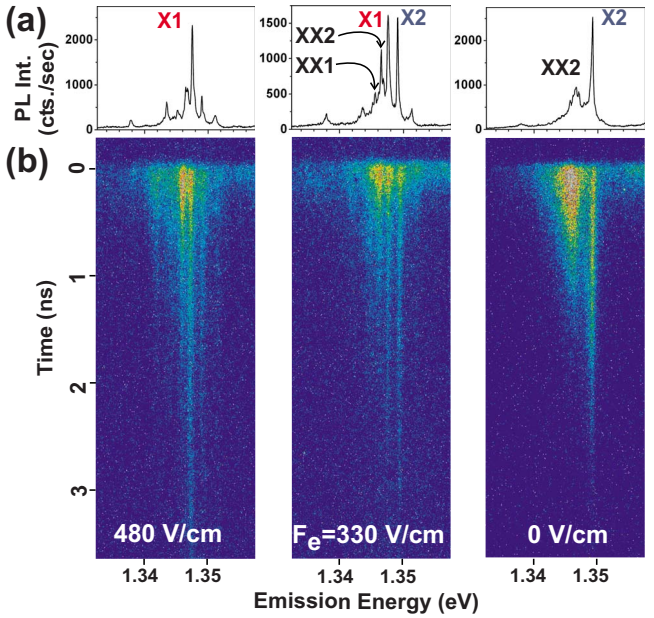

FIG. 2. (Color online) (a) Time-integrated PL spectra of a single QDM for the different alignment situations at three different electric field strengths, F=480 V/cm, $F=F_e$=330 V/cm (alignment case), and F=0 V/cm. (b) The corresponding time-energy-resolved Streak camera images.

time-integrated PL spectra of a single lateral QDM under nonresonant 3 ps pulsed laser excitation were recorded using a charge coupled device camera [Fig. 2(a)]. The time-resolved spectra were acquired as summations of 200 background-corrected 10 s exposures using a streak camera [Fig. 2(b)]. Although typical count rates of a few thousand per second could be achieved for the detected QDM PL and a large number of background-corrected images were accumulated, the experiments have been carried out close to the signal limit of the streak camera photocathode, which is determined by its noise (500 electrons cm$^{-2}\times$s) and quantum efficiency in the spectral range under investigation ($<$0.05% at 1.35 eV).

The electrical tuning of the QDM charge distribution and optical emission properties was performed via a lateral electric field. The field was applied along the coupling axis between the two dots, [1$\bar{1}$0], through the parallel gold electrodes as described in detail in Refs. 17 and 22.

III. EXPERIMENTAL RESULTS

The effect of changing the lateral electric field along the molecular coupling axis on the QDM PL spectrum is displayed in Fig. 2(a). At the electron alignment field, F_e, the electron is completely delocalized over both dots which corresponds to a regime of resonant electron tunneling. When a hole is added to one of the dots composing the QDM, the Coulomb binding energy leads to the formation of a lower energy direct and a higher energy indirect exciton, with an energetic separation of around 10 meV, as schematically illustrated in Fig. 3. This energy separation suppresses the resonant tunneling, which is possible for an isolated electron.

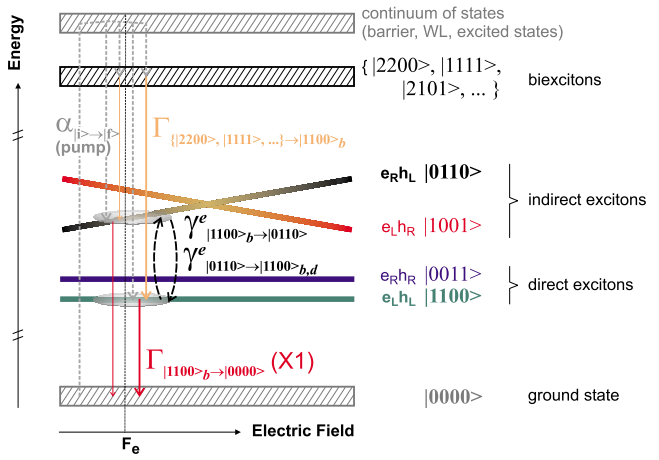

FIG. 3. (Color online) Schematic level diagram illustrating the molecular states, the pump, recombination and tunnel rates, and the nomenclature that is used in the model.

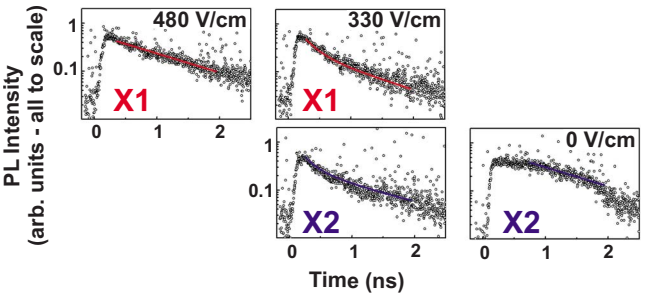

FIG. 4. (Color online) PL time traces of the nonresonantly excited QDM displayed in Fig. 2, featuring the excitonic recombination X1 (left panel), X1 and X2 (center panel at F_e), and X2 (right panel) including guides to the eye, to highlight the decay behavior. The time, traces are integrated over 16 channels on the energy axis of the Streak camera data, which corresponds to a spectral range of 0.5 meV.

The two possible radiative decay channels can therefore be identified as direct neutral exciton recombination in one of the two coupled dots, resulting in the two recombination peaks X1 and X2. The difference in their absolute emission energy is due to small variations in dot dimensions, composition, strain, etc. The single-particle picture is chosen here for simplicity to illustrate, first, the possible separate treatment of the direct and indirect exciton configurations, which do not mix or anticross within the investigated electric field range. Second, the separate tunneling of the electron and hole with significantly different rates is highlighted in this picture. This difference leads to effective transitions between indirect and direct excitons. The indirect excitonic configurations, with the electron and hole located in different dots, exhibit much smaller oscillator strengths due to the drastically reduced spatial overlap of their wave functions when compared to the direct case. Consequently, they are essentially optically inactive, which is in contrast to vertically coupled QDs, where the indirect excitonic recombination is, although weaker, usually visible due to a still substantial oscillator strength.

The time traces for the direct excitons X1 and X2 are displayed in Fig. 4. A clear difference is visible in the excitonic decay behavior for the three tuning situations. In the two "misalignment cases," where one of the neutral excitons dominates the spectrum (left and right panels), monoexponential decay at rates of 1.2 ± 0.3 ns^{-1}, which are typical for the investigated dot structures, sets in after a slight delay (plateau), similar to a single-dot exciton in a radiative biexciton-exciton cascade. The plateau is more pronounced for the 0 V/cm data because of the slightly higher excitation power and thus more likely pumping of the exciton state via the corresponding radiative biexciton-exciton cascade. In contrast to these two cases the alignment case at F_e (central panel) exhibits a clear deviation from a single-dotlike situation and reveals an over all faster double-exponential-like decay which is attributed to two different mechanisms, nonradiative filling and decay via charge carrier tunneling as well as radiative recombination; this process will be discussed qualitatively in more detail in Sec. V. All the time traces, especially in the alignment case, seem to exhibit a slower decay component or delayed filling at larger times, which is again attributed to charge carrier tunneling.

Comparing these situations it becomes obvious that the dynamical processes leading to the exciton formation, molecular tunnel-coupling and exciton decay in the lateral QDMs clearly manifest themselves in the temporal evolution of the QDM emission. In the subsequent sections, a model is introduced to explain these mechanisms and to fit the data, followed by a discussion of possible underlying physical mechanisms.

IV. SIMULATION

A rate equation model has been developed for the lateral QDMs in order to describe the charge carrier dynamics and the decay behavior of the bright exciton states. The model accounts for the dynamics of excitons, radiative cascades, and spin-flip processes in single dots,[23–26] as well as the tunneling processes reported in stacked asymmetric double dots.[27,28] It also includes all neutral and singly charged s-shell single-particle configurations and can therefore be used to model the dynamics of excitons, charged excitons, and biexcitons. The nomenclature used for the various states and rates is outlined in the Table I and in Fig. 3. The states are $|Ne_L, Nh_L, Ne_R, Nh_R\rangle$ with $Ne(h)=0,\ldots,2$ describing the number of electrons (holes) and L,R indicating the left and right dots, respectively. The carrier capture rates are $\alpha_{|i\rangle\rightarrow|f\rangle}$, the radiative rates are $\Gamma_{|i\rangle\rightarrow|f\rangle}$, where i,f indicate the initial and final states of the transition. The effect of Coulomb and spin interactions on the charge carrier and exciton dynamics is included via the related tunnel rates that correspond to an effective hopping of the electron (hole), $\gamma^{e(h)}_{|i\rangle\rightarrow|f\rangle}$, and the spin-flip rates, $\gamma^{s}_{|i\rangle_b\rightarrow|f\rangle_d} = \gamma^{s}_{|i\rangle_d\rightarrow|f\rangle_b}$, where b,d indicate the bright and dark direct excitons.

An initially empty QDM is nonresonantly excited using a 3 ps laser pulse that is absorbed in the GaAs barrier or WL. According to the dynamical scenario for the charge carrier capture into the QDM under nonresonant excitation that is discussed in detail in Ref. 21 the generated electrons, holes,

TABLE I. Nomenclature of the states and parameters used in the simulation. The most relevant rates are given including the used values that were obtained from own experiments or literature.

State/parameter	Description and comments	Type[a]	F (V/cm)	Value, unit
$\lvert Ne_L, Nh_L, Ne_R, Nh_R\rangle$	General form of a QDM state with the number of electrons (holes), $Ne_{L,R}(Nh_{L,R})$, in the left, right dots			
For example, $\lvert 1100\rangle_{b,d}$	Direct exciton in the left dot with b,d indicating the optically bright and dark configurations			
$\lvert 1001\rangle$	Indirect exciton with e in the left and h in the right dot			
$\Gamma_{\lvert i\rangle\rightarrow\lvert f\rangle}$	Radiative recombination rate from initial state $\lvert i\rangle$ to final state $\lvert f\rangle$			
$\Gamma_{\lvert 1100\rangle_b\rightarrow\lvert 0000\rangle}$, $\Gamma_{\lvert 0011\rangle_b\rightarrow\lvert 0000\rangle}$	Bright exciton recombination X1, X2	Exp.	0	1.2 ns^{-1}
			330	1.7 ns^{-1}
			480	1.3 ns^{-1}
$\Gamma_{\lvert 2200\rangle\rightarrow\lvert 1100\rangle_b}$, $\Gamma_{\lvert 0022\rangle\rightarrow\lvert 0011\rangle_b}$	Biexciton recombination XX1, XX2	Exp.	0	2.5 ns^{-1}
			330	2.9 ns^{-1}
			480	2.3 ns^{-1}
$\Gamma_{\lvert 2100\rangle\rightarrow\lvert 1000\rangle}$	Negative trion recombination	Exp.		2 ns^{-1}
$\Gamma_{\lvert 1200\rangle\rightarrow\lvert 0100\rangle}$	Positive trion recombination	Exp.		2 ns^{-1}
$\gamma_{\lvert i\rangle\rightarrow\lvert f\rangle}$	Spin-flip/tunnel rate from initial state $\lvert i\rangle$ to final state $\lvert f\rangle$			
$\gamma^s_{\lvert 1100\rangle_b\rightarrow\lvert 1100\rangle_d}=\gamma^s_{\lvert 1100\rangle_d\rightarrow\lvert 1100\rangle_b}$	Spin-flip rate, bright$\rightarrow$dark exciton=dark$\rightarrow$bright exciton	Ref. 25		0.05 ns^{-1}
$\gamma^e_{\lvert 1100\rangle_b\rightarrow\lvert 0110\rangle}$	Tunneling from a direct bright initial configuration =effective electron hopping	Sim.		
$\gamma^h_{\lvert 1100\rangle_b\rightarrow\lvert 1001\rangle}$	Tunneling from a direct bright initial configuration =effective hole hopping	Sim.		
$\gamma^e_{\lvert 0110\rangle\rightarrow\lvert 1100\rangle}$	Tunneling from an indirect initial configuration=effective electron hopping	Sim.		
$\gamma^h_{\lvert 1001\rangle\rightarrow\lvert 1100\rangle}$	Tunneling from an indirect initial configuration=effective hole hopping	Sim.		
$\alpha_{\lvert i\rangle\rightarrow\lvert f\rangle}$	Capture rate=generation rate of state $\lvert f\rangle$ from state $\lvert i\rangle$ rates assumed due to carrier drift and diffusion velocities, the excitation volume and Refs. 29 and 30			
$\alpha_{\mathrm{WL}\rightarrow\lvert 1100\rangle_b}$	Bright exciton capture rate			>10 ns^{-1}
$\alpha_{\mathrm{WL}\rightarrow\lvert 1000\rangle}$	Electron capture rate	Ref. 21		$\gg\alpha_{\mathrm{WL}\rightarrow\lvert 1100\rangle_b}$
$\alpha_{\mathrm{WL}\rightarrow\lvert 0100\rangle}$	Hole capture rate	Ref. 21		$<\alpha_{\mathrm{WL}\rightarrow\lvert 1000\rangle}$

[a]"Type:" obtained from own experiment (Exp.), from a reference (Ref.) or used as simulation parameter (Sim.)—with the values and ranges given in the insets of Fig. 5; electric fields "F" and "Values, units" as used in the simulation.

and excitons can either recombine at a rate of $\Gamma_{\{barrier,\mathrm{WL}\}} \geq 10$ ns^{-1} or relax to the QDM states that are approximately 40–70 meV lower in energy at comparable rates of $\alpha_{\{barrier,\mathrm{WL}\}\rightarrow\lvert i\rangle} > 10$ ns^{-1}.

The following rate equation system was solved to describe the exciton dynamics:

$$\frac{d}{dt}P_{\lvert i\rangle}(t) = -\sum_{j,k}\{\Gamma_{\lvert i\rangle\rightarrow\lvert j\rangle}\cdot P_{\lvert i\rangle}(t) + \gamma_{\lvert i\rangle\rightarrow\lvert k\rangle}\cdot P_{\lvert i\rangle}(t)\} + \sum_{l,m,n}\{\Gamma_{\lvert l\rangle\rightarrow\lvert i\rangle}\cdot P_{\lvert l\rangle}(t)[1-P_{\lvert i\rangle}(t)] + \alpha_{\lvert m\rangle\rightarrow\lvert i\rangle}\cdot P_{\lvert m\rangle}(t) + \gamma_{\lvert n\rangle\rightarrow\lvert i\rangle}\cdot P_{\lvert n\rangle}(t)\}$$

with the sum of all QDM states obeying the normalization condition $\Sigma_i P_{\lvert i\rangle}(t)=1$. The temporal evolution of the state $\lvert i\rangle$ is described via its population $P_{\lvert i\rangle}(t)$. The first sum describes all processes leading to a population reduction in the state $\lvert i\rangle$, i.e., the radiative decay processes with the rates $\Gamma_{\lvert i\rangle\rightarrow\lvert j\rangle}$ and the tunnel and spin-flip processes with the rates $\gamma_{\lvert i\rangle\rightarrow\lvert k\rangle}$. The second sum describes all processes leading to a population enhancement of the state $\lvert i\rangle$, i.e., the radiative decay processes of the state $\lvert l\rangle$ with the rate $\Gamma_{\lvert l\rangle\rightarrow\lvert i\rangle}$, e.g., in a biexciton-exciton cascade, the charge carrier capture processes with the rates $\alpha_{\lvert m\rangle\rightarrow\lvert i\rangle}$ and the tunnel and spin-flip processes with the rates $\gamma_{\lvert n\rangle\rightarrow\lvert i\rangle}$.

The electric field tuning is included as a linear weighting factor of the capture (α) and tunnel (γ) rates. When the QDM is in the alignment case the carrier capture rates into the left and right dots are equal (1:1 weighting between left and right dot rates) and all direct and indirect excitons are formed, i.e., $\lvert 1100\rangle$, $\lvert 0011\rangle$, $\lvert 1001\rangle$, and $\lvert 0110\rangle$. When the QDM is in one of the misalignment cases the capture rates into the two dots are different (0.1:1 weighting) which correspond to a suppression of the weaker excitonic transition of about one order of magnitude with respect to the dominant

one. This ratio is in good agreement with the experimental results recorded from dozens of QDMs as a function of electric field. Direct exciton formation dominates in the individual dots of a single QDM as a result of the different rates at which the single-charge carrier capture processes take place.[21] The carrier capture and relaxation occurs at faster rates for the electron than the hole, e.g., the electron capture rate into the left dot is larger than the corresponding hole rate, $\alpha_{\mathrm{WL}\rightarrow|1000\rangle} > \alpha_{\mathrm{WL}\rightarrow|0100\rangle}$. Initially, this can lead to a preferential electron occupation of either dot, where the electron position is controllable and a function of the applied lateral electric field. This electron "positioning" can, in turn, enhance the hole capture by the same dot due to Coulomb attraction.

The radiative decay rates could be obtained from experiments and are between 1.2 and 1.7 ns^{-1} for the direct excitons and between 2.3 and 2.9 ns^{-1} for the biexcitons. The spin-flip rate between the bright and dark excitonic configurations is assumed to be small compared to all other rates and equal in both directions.[25] The indirect and dark exciton recombination rates are set one order of magnitude smaller than the corresponding direct and bright exciton rates, following the argument of a reduced oscillator strength for the indirect excitons and a reduced probability of a spin-forbidden recombination.[26,28] The exact values of these rates are not critical to the simulation results as long as they remain small.

The energetic separation of indirect and direct excitons leads to different tunneling rates whose magnitudes depend on whether the phonon-assisted processes require the emission or absorption of an acoustic phonon and on the phonon density of states as well as relative momenta. At the experimental low-temperature conditions, phonon-emission processes are possible as long as the total energy matches the acoustic phonon branch, which should be the case when $\Delta E \leq \hbar\omega_{\mathrm{TA}}^{\mathrm{GaAs}} \approx 9.9$ meV. Phonon-absorption processes, however, depend on the thermal energy of the lattice, which consequently leads to the assumption that tunneling processes that require the absorption of a phonon must be significantly suppressed. In contrast to reports on coherent tunneling in asymmetric double dots[27] and the coherent tunneling which would be possible for a single electron at F_e in a lateral QDM, the tunneling between direct and indirect excitons which is described here is a nonresonant process and thus not coherent.

The only simulation parameters used in the model calculations are the tunneling rates between direct and indirect excitons, i.e., effective hopping processes of electrons (e.g., $\gamma^e_{|0110\rangle\rightarrow|1100\rangle}$) and holes (e.g., $\gamma^e_{|0110\rangle\rightarrow|0011\rangle}$). According to previous reports[20,21] all tunnel rates that correspond to an effective hopping of the hole are set to smaller values (1%) compared to the rates that correspond to an effective hopping of the electron following the aforementioned arguments. All other rates are fixed because they can be either taken according to different own experiments or literature or they are small and thus negligible.

Figures 5(a) and 5(b) compare the simulation scenarios of the X1 PL intensity, $\Gamma_{|1100\rangle_b\rightarrow|0000\rangle} \times P_{|1100\rangle_b}(t)$, where the effect of phonon emission or absorption processes on the tunnel rates is (a) not included to those where it is (b) included

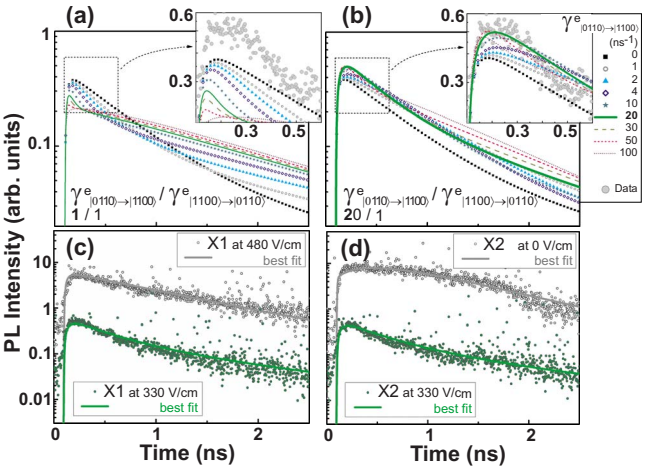

FIG. 5. (Color online) The simulation results for the direct exciton, X1, are displayed at $F_e = 330$ V/cm with the electron tunnel rate from an indirect exciton configuration varied between 0 and 100 ns^{-1}. The tunnel rate ratios are set as follows: (a) (initially indirect:direct exciton)=(1:1) and (b) (20:1), the values of $\gamma^e_{|0110\rangle\rightarrow|1100\rangle}$ are given as inset. The simulation results with best-fit parameters (lines) vs experimental data (symbols) for (c) X1 and (d) X2 at the different alignment conditions.

using a ratio of 20:1 between processes that require the emission to those that require the absorption of a phonon. This corresponds to the ratio between tunnel rates from indirect and direct initial configurations, e.g., $\gamma^e_{|0110\rangle\rightarrow|1100\rangle} / \gamma^e_{|1100\rangle\rightarrow|0110\rangle} = 20$. Figure 5(a) clearly shows that none of the simulation results fits the data due to the fast decay of the bright direct exciton population at small times (inset) and the overly too slow decay at longer times, which is the result of a balanced tunneling between the different Coulomb interaction configurations (direct/indirect exciton). Figure 5(b) demonstrates that it becomes possible to fit the experimental data when Coulomb interactions are included in the simulation in terms of different tunnel rates depending on the initial-state character and the related phonon emission or absorption process. The best-fit curve (bold green line) for the X1 bright exciton recombination, $\Gamma_{|1100\rangle_b\rightarrow|0000\rangle} \times P_{|1100\rangle_b}(t)$, is obtained for the following tunnel rates, i.e., electron hopping rates: $\gamma^e_{|0110\rangle\rightarrow|1100\rangle} = 20\ \mathrm{ns}^{-1}$ and $\gamma^e_{|1100\rangle\rightarrow|0110\rangle} = 1\ \mathrm{ns}^{-1}$. Figures 5(c) and 5(d) show that the model can describe both the alignment and misalignment cases. The experimental data and simulation results obtained with the best-fit parameter set are displayed for the different electric field tuning situations. The X1 recombination, $\Gamma_{|1100\rangle_b\rightarrow|0000\rangle} \times P_{|1100\rangle_b}(t)$, is presented in Fig. 5(c) where the upper curve reveals the single-dotlike decay below optical saturation in the misalignment case (gray) and the lower curve presents the alignment case (green). The X2 recombination, $\Gamma_{|0011\rangle_b\rightarrow|0000\rangle} \times P_{|0011\rangle_b}(t)$, is presented in Fig. 5(d) where the misalignment case is taken at slightly higher excitation power density leading to the onset of a plateau due to the biexciton-exciton cascaded recombination and saturation effects, which also become visible in the simulation result (gray). The lower curve, again, presents the alignment case (green).

V. DISCUSSION

The postulated explanation for the observed PL time dependence is a combination of the particular charge carrier capturing process, with larger rates for the electron as compared to the hole, and the phonon-mediated asymmetric charge carrier tunneling process. Regarding one particular exciton state of interest, e.g., the direct exciton $|1100\rangle$, such charge carrier tunneling affects the population of this state, which is observed as the initial state involved in a radiative recombination process, e.g., the direct exciton recombination X1, in two different ways. First, the population of this state can be enhanced due to the nonradiative decay of another state into this state of interest, such as, the hopping of an electron, which consequently leads to an enhancement of the PL intensity of the corresponding radiative recombination. This is the case for the fast decay of indirect excitons via electron hopping that enhances the population of the direct excitons on a very short time scale after the excitation event. Second, the population of the state of interest can be reduced due to a nonradiative decay (hopping of a charge carrier) into another state, which leads to a reduction in the PL intensity of the respective radiative recombination of this state. These bidirectional tunneling processes manifest themselves in the deviation from a simple monoexponential decay of the PL of the radiative level and feature the observed double-exponential-like decay, which can no longer be expressed in terms of a state decaying exponentially with a single rate given as the sum of all contributing decay processes.

It has to be noted, however, that the molecular exciton decay behavior presented here, although quite clear and pronounced, has not been observed for all of the investigated QDMs. For a particular class of molecules that exhibit their alignment at comparable and small electric fields on the order of $F_e = 0 \pm 500$ V/cm the effects discussed above were observed while in some measurements performed on different QDMs with larger $|F_e|$ it could not be observed. The reason for this could be the dominance of the quantum-confined Stark effect at larger fields that could lead to quenching of the charge carrier tunneling and tuning ability which is responsible for the characteristic PL decay. However, to date the most likely explanation is the aforementioned phonon-mediated asymmetric charge carrier tunneling, which is expected to strongly depend on the level structure of the investigated QDM and the acoustic phonon spectra. When the energy separations between correlated indirect and direct excitons are not covered by the acoustic phonon branch no such tunneling can occur. It is reasonable to assume that the effective carrier hopping that requires a distinct momentum transfer is more efficient for larger energy separations and thus for QDMs with a rather small alignment field F_e. This is due to the higher phonon density of states at higher energies close to the transverse acoustic phonon energy of $\hbar\omega_{\mathrm{TA}}^{\mathrm{GaAs}}(X) \approx 9.9$ meV.

VI. SUMMARY

In summary, we present the charge carrier dynamics in a lateral QDM under the influence of an external electric field under nonresonant pulsed optical excitation. We have found that the molecular Coulomb interactions have an essential impact on the temporal evolution of the charge carrier distribution and dynamics. The experimentally obtained time-resolved spectra exhibit a characteristic decay behavior which depends on the excitation power and especially on the applied lateral electric field. Under higher power excitation, due to the initial creation of two (or more) electron-hole pairs, a plateau is observed in the neutral direct exciton PL decay. It is the direct consequence of the corresponding radiative biexciton-exciton cascade and the repopulation of the radiative level at shorter time scales. Under lower power excitation the plateau vanishes. The direct exciton PL decay can furthermore be varied depending on the applied lateral electric field that tunes the spatial distribution of the charge carriers in the QDM. At the electron alignment field, F_e, the decay of the direct exciton features a clear deviation from a monoexponential decay, with a pronounced fast component, which is attributed to electron hopping between indirect and direct exciton configurations. Using a rate equation model, including the relevant processes occurring in the lateral QDM system, the exciton dynamics could be modeled. The proposed asymmetric tunnel process between indirect and direct excitonic configurations could be confirmed with a 20 times faster tunneling from an indirect to a direct exciton. We therefore suggest that nonresonant acoustic phonon-mediated tunneling is the source of the observed characteristic time evolution of the presented lateral QDM excitonic spectrum. Such an understanding and control of the spectral and temporal properties represents a first step toward the realization of a fast optical quantum gate based on a lateral QDM.

ACKNOWLEDGMENTS

The authors thank M. Wiesner, W.-M. Schulz, M. Eichfelder, R. Rossbach, M. Jetter, and M. Ubl for assistance during sample growth and processing. Work at the University of Stuttgart was financially supported by the Deutsche Forschungsgemeinschaft via SFB/TRR 21 and FOR 730.

*Present address: Research Institute for Electronic Science (RIES), Hokkaido University, Sapporo 001-0021, Japan; claus@es.hokudai.ac.jp

†Present address: The Cavendish Laboratory, University of Cambridge, J. J. Thomson Ave., Cambridge CB3 0HE, UK.

[1] *Single Semiconductor Quantum Dots*, NanoScience and Technology, edited by P. Michler (Springer, Berlin, 2009).

[2] P. Michler, A. Kiraz, C. Becher, W. V. Schoenfeld, P. M. Petroff, L. D. Zhang, E. Hu, and A. Imamoglu, Science **290**, 2282 (2000).

[3] R. M. Stevenson, R. J. Young, P. Atkinson, K. Cooper, D. A. Ritchie, and A. J. Shields, Nature (London) **439**, 179 (2006).

[4] N. Akopian, N. H. Lindner, E. Poem, Y. Berlatzky, J. Avron, D. Gershoni, B. D. Gerardot, and P. M. Petroff, Phys. Rev. Lett. **96**, 130501 (2006).
[5] R. Hafenbrak, S. M. Ulrich, P. Michler, L. Wang, A. Rastelli, and O. G. Schmidt, New J. Phys. **9**, 315 (2007).
[6] N. H. Bonadeo, J. Erland, D. Gammon, D. Park, D. S. Katzer, and D. G. Steel, Science **282**, 1473 (1998).
[7] X. Q. Li, Y. W. Wu, D. Steel, D. Gammon, T. H. Stievater, D. S. Katzer, D. Park, C. Piermarocchi, and L. J. Sham, Science **301**, 809 (2003).
[8] G. S. Solomon, J. A. Trezza, A. F. Marshall, and J. S. Harris, Phys. Rev. Lett. **76**, 952 (1996).
[9] M. Bayer, P. Hawrylak, K. Hinzer, S. Fafard, M. Korkusinski, Z. R. Wasilewski, O. Stern, and A. Forchel, Science **291**, 451 (2001).
[10] H. J. Krenner, M. Sabathil, E. C. Clark, A. Kress, D. Schuh, M. Bichler, G. Abstreiter, and J. J. Finley, Phys. Rev. Lett. **94**, 057402 (2005).
[11] G. Ortner, M. Bayer, Y. Lyanda-Geller, T. L. Reinecke, A. Kress, J. P. Reithmaier, and A. Forchel, Phys. Rev. Lett. **94**, 157401 (2005).
[12] E. A. Stinaff, M. Scheibner, A. S. Bracker, I. V. Ponomarev, V. L. Korenev, M. E. Ware, M. F. Doty, T. L. Reinecke, and D. Gammon, Science **311**, 636 (2006).
[13] H. J. Krenner, E. C. Clark, T. Nakaoka, M. Bichler, C. Scheurer, G. Abstreiter, and J. J. Finley, Phys. Rev. Lett. **97**, 076403 (2006).
[14] M. Scheibner, I. V. Ponomarev, E. A. Stinaff, M. F. Doty, A. S. Bracker, C. S. Hellberg, T. L. Reinecke, and D. Gammon, Phys. Rev. Lett. **99**, 197402 (2007).
[15] O. G. Schmidt, C. Deneke, S. Kiravittaya, R. Songmuang, H. Heidemeyer, Y. Nakamura, R. Zapf-Gottwick, C. Müller, and N. Y. Jin-Phillipp, IEEE J. Sel. Top. Quantum Electron. **8**, 1025 (2002).
[16] R. Songmuang, S. Kiravittaya, and O. G. Schmidt, Appl. Phys. Lett. **82**, 2892 (2003).
[17] G. J. Beirne, C. Hermannstädter, L. Wang, A. Rastelli, O. G. Schmidt, and P. Michler, Phys. Rev. Lett. **96**, 137401 (2006).
[18] L. Robledo, J. Elzerman, G. Jundt, M. Atature, A. Hogele, S. Falt, and A. Imamoglu, Science **320**, 772 (2008).
[19] G. Bester, J. Shumway, and A. Zunger, Phys. Rev. Lett. **93**, 047401 (2004).
[20] L. Wang, A. Rastelli, S. Kiravittaya, P. Atkinson, F. Ding, C. C. B. Bufon, C. Hermannstädter, M. Witzany, G. J. Beirne, P. Michler, and O. G. Schmidt, New J. Phys. **10**, 045010 (2008).
[21] J. Peng, C. Hermannstädter, M. Witzany, M. Heldmaier, L. Wang, S. Kiravittaya, A. Rastelli, O. G. Schmidt, P. Michler, and G. Bester, Phys. Rev. B **81**, 205315 (2010).
[22] C. Hermannstädter, M. Witzany, G. J. Beirne, W.-M. Schulz, M. Eichfelder, R. Rossbach, M. Jetter, P. Michler, L. Wang, A. Rastelli, and O. G. Schmidt, J. Appl. Phys. **105**, 122408 (2009).
[23] V. Zwiller, M.-E. Pistol, D. Hessman, R. Cederström, W. Seifert, and L. Samuelson, Phys. Rev. B **59**, 5021 (1999).
[24] E. Dekel, D. V. Regelman, D. Gershoni, E. Ehrenfreund, W. V. Schoenfeld, and P. M. Petroff, Phys. Rev. B **62**, 11038 (2000).
[25] G. A. Narvaez, G. Bester, A. Franceschetti, and A. Zunger, Phys. Rev. B **74**, 205422 (2006).
[26] M. Reischle, G. J. Beirne, R. Roßbach, M. Jetter, and P. Michler, Phys. Rev. Lett. **101**, 146402 (2008).
[27] J. M. Villas-Bôas, A. O. Govorov, and S. E. Ulloa, Phys. Rev. B **69**, 125342 (2004).
[28] M. Reischle, G. J. Beirne, R. Roßbach, M. Jetter, H. Schweizer, and P. Michler, Phys. Rev. B **76**, 085338 (2007).
[29] T. C. Damen, L. Vina, J. E. Cunningham, J. Shah, and L. J. Sham, Phys. Rev. Lett. **67**, 3432 (1991).
[30] T. Müller, F. F. Schrey, G. Strasser, and K. Unterrainer, Appl. Phys. Lett. **83**, 3572 (2003).